Magnetic reconnection in the high-energy density regime

IOP Publishing Plasma Physics and Controlled Fusion
Plasma Phys. Control. Fusion 59 (2017) 064002 (6pp) https://doi.org/10.1088/1361-6587/aa6803

Magnetic reconnection in the high-energy density regime

B Qiao[1,2,4], Z Xu[1,4], W P Yao[1,4], H X Chang[1,4] and X T He[3,4]

[1] HEDPS, Center for Applied Physics and Technology, & School of Physics, Peking University, Beijing 100871, People's Republic of China
[2] Collaborative Innovation Center of Extreme Optics, Shanxi University, Taiyuan, Shanxi 030006, People's Republic of China
[3] Institute of Applied Physics and Computational Mathematics, Beijing 100094, People's Republic of China
[4] Collaborative Innovation Center of IFSA (CICIFSA), Shanghai Jiao Tong University, Shanghai 200240, People's Republic of China

E-mail: bqiao@pku.edu.cn

Received 31 October 2016, revised 18 March 2017
Accepted for publication 21 March 2017
Published 19 April 2017

Abstract

Magnetic reconnection (MR) in the high-energy-density (HED) regime is comprehensively investigated by particle-in-cell simulations. In the HED regime, the MR process is driven by two colliding magnetized plasma bubbles produced by intense lasers, where there are ambiguities in distinguishing the actual MR consequences from the pure bubble squeezing effects, because both lead to similar behaviors. After discerning these similarities, such as two-fluid effects, plasma heating and jetting, we establish the direct relevance between the actual consequences of MR with the electron dissipation region, magnetic energy conversion and the relaxation of plasma density gradient. With additional discussions of the 3D effects and relativistic features, the results will guide the future HED experiments for MR and other laboratory astrophysics studies.

Keywords: magnetic reconnection, high-energy density, particle-in-cell simulation

(Some figures may appear in colour only in the online journal)

1. Introduction

Magnetic reconnection (MR) is believed to be the engine of many space and astrophysical explosive processes [1–3]. As a result of breaking and reorganizing the magnetic field lines, the stored magnetic energy is suddenly released in bursts of kinetic and thermal energy. Although this process has puzzled us for more than half a century, recent years have witnessed great progress in the understanding of MR in traditional plasmas (tenuous, quasi-steady, cold, where the thermal pressure in plasmas is smaller than the magnetic pressure, i.e. $\beta = 2n_0\mu_0 T_{e0}/B_0^2 < 1$), which exist in the solar corona [4], Earth's magnetosphere [5], and laboratory experiment facilities (e.g., The Magnetic Reconnection Experiment [6]).

These successes now drive a new trend of MR research towards a wider regime [7], where various explosive astrophysical phenomena with high plasma β are related with [2, 3]. Comparing with the traditional MR, inherent distinctions are found when plasma $\beta > 1$, e.g., the magnetic fields are compressed by the forced plasma flows. In order to identify the key roles these differences play in MR, recently, numerous MR studies have been carried out under a new platform—high-energy-density (HED) laser-plasma experiments, where similar distinguishing features exist, i.e. strongly forced inflows with the thermal pressure dominating the magnetic pressure ($\beta > 1$) [8]. In these laboratory MR studies [9–14], by irradiating a solid target with two lasers, two magnetized HED plasma bubbles are produced and then they expand freely until contacting with each other. When the attached opposite magnetic fields (generated by Biermann battery effect) are squeezed in the colliding center, the MR process occurs.

Although abundant results are diagnosed during these experiments: the decreasing of magnetic flux [10, 13]; heating of electrons [9, 13]; generating of jets [9] and ejecting of plasmoids [12], it is challenging to establish a direct relevance between these diagnoses and the real MR results. This is because there are ambiguities, as pointed out in [15], to

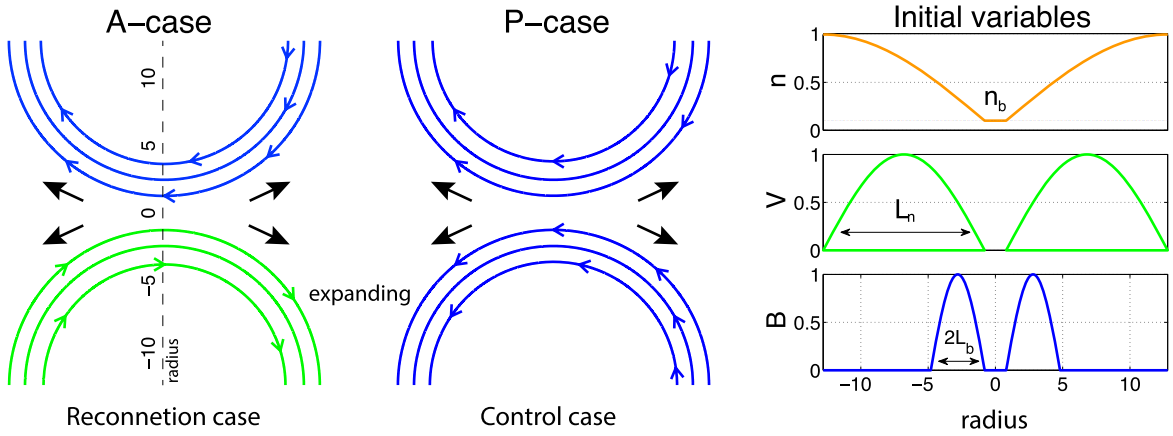

Figure 1. Initial particle-in-cell simulation setup: modeling for the two expanding plasma bubbles carrying antiparallel and parallel magnetic field ribbons, named respectively as the A- and P-cases. The plots show the initial variables of density n, radial expanding velocity V, and magnetic field B versus radius, normalized by n_0, V_0, B_0 and d_i, respectively. Detailed simulation parameters are shown in the text.

distinguish the MR impacts from the bubble collision effects; both can lead to similar behaviors: plasmas enter into the colliding center and then flows are squeezed out from two lateral sides of the bubble ribbons. The resulting motion will give rise to diagnoses like two-fluid effects, heating and jetting, which are traditionally considered as the evidence of MR. Our previous study has shown the key sign of MR is the occurrence of a dissipation region by a comparative study with two cases [15], one with anti-parallel and the other with parallel magnetic field configuration.

However, a natural question arises—besides the diagnoses of the MR experiments, what is the actual MR results, and what is their relation with the impacts of colliding bubbles? In this paper, before identifying the real MR consequences, ambiguities are discerned first in the particle-in-cell (PIC) simulations. Then the MR impacts are recognized: the dissipation of magnetic energy, acceleration of particles and relaxation of density gradient. Finally, we discuss the 3D effects and the relativistic features, which are more related to these laboratory studies and will present more challenges in future research.

2. Simulation setup

We perform two cases, A- and P-case, by a relativistic PIC code 'EPOCH' [16]. There is a benefit to employ two such cases [15], one with antiparallel magnetic field configurations (named as A-case) and the other with parallel field (P-case), shown in figure 1. The initial setup is similar to that used in [8, 17, 18], where two magnetized plasma bubbles are prescribed to mimic a laser-produced state. As shown in figure 1, two identical semicircular plasma bubbles are wrapped up with magnetic ribbon. They only differ in the azimuthal direction of magnetic field, which is feasible in experiments [11, 19]. Specifically, the two half-bubbles are located at $(0, L_y)$ and $(0, -L_y)$ with radius vectors of $\boldsymbol{r}^{(1)} = (x, y + L_y)$ and $\boldsymbol{r}^{(2)} = (x, y - L_y)$, respectively. The bubbles are set up with the initial density $n = n^{(1)} + n^{(2)} + n_b$, expansion velocity $\boldsymbol{V} = \boldsymbol{V}^{(1)} + \boldsymbol{V}^{(2)}$, and the magnetic field $\boldsymbol{B} = \boldsymbol{B}^{(1)} + \boldsymbol{B}^{(2)}$, where

$$n^{(i)} = (n_0 - n_b)\cos^2(\pi r^{(i)}/2L_n)H_1, \ (i = 1, 2) \tag{1}$$

$$\boldsymbol{V}^{(i)} = V_0 \sin(\pi r^{(i)}/L_n)\hat{\boldsymbol{r}}^{(i)}H_1, \tag{2}$$

$$\boldsymbol{B}^{(i)} = B_0 \sin[\pi(L_n - r^{(i)})/2L_b]\hat{\boldsymbol{r}}^{(i)} \times \hat{\boldsymbol{z}}H_2, \tag{3}$$

and n_0, n_b, V_0, and B_0 are the initial parameters. In addition, $H_1 = H(L_n - r^{(i)})$ and $H_2 = H([r^{(i)} - (L_n - 2L_b)](L_n - r^{(i)}))$ are the Heaviside step functions, where L_n is the bubble radius and L_b is the half-width of the ribbons. The 3D cases are similar, but with a hemisphere-extension and a cylinder-extension in the z-direction.

In order to match the experiments and to reduce the numerical calculation, we choose the parameters here to be similar to those in [15]. The simulation box size is taken as $L_x \times L_y = 51.2d_\mathrm{i} \times 25.6d_\mathrm{i}$ ($L_z = 12.8d_\mathrm{i}$ in 3D), where $d_\mathrm{i} = c/\omega_\mathrm{pi}$ is the ion skin depth, c is the light speed and ω_pi is the ion oscillation frequency. The bubble radius and ribbon width are $L_\mathrm{n} = 12d_\mathrm{i}$ and $L_\mathrm{b} = 2d_\mathrm{i}$, respectively. We choose the background density $n_\mathrm{b} = 0.1n_0$, the plasma beta $\beta_\mathrm{e} = 2n_0\mu_0T_\mathrm{e0}/B_0^2 = 5$ and the Alfvén speed $V_\mathrm{A} = c/100$, where μ_0 is the vacuum permeability, and T_e0 is the initial electron temperature. The bubble expansion velocity is $V_0 = 2.0C_\mathrm{s}$, where C_s is the sound speed with the defined adiabatic coefficient $5/3$. Correspondingly, the ram pressure is $\beta_\mathrm{ram} = \frac{1}{2}\rho V_0^2/(B^2/2\mu_0) \approx 16.5$. In order to model a large space scale and the nanosecond physics, we use a low ion-electron mass ratio $m_\mathrm{i}/m_\mathrm{e} = 100$, and a high initial temperature $T_0 = T_\mathrm{e0} = T_\mathrm{i0} = 0.025m_\mathrm{e}c^2$ in the PIC simulations, hence, the computation scales are reduced. Spatially 1024×512 ($\times 256$ in 3D) cells are employed with 144 (8 in 3D) particles per cell in the simulations. Reflecting boundary conditions for particles and conducting boundary conditions for fields are employed.

For convenience, simulation results in the following are presented in the normalized units: density to n_0, velocity to c, magnetic field to B_0, length to d_i, time to the ion cyclotron frequency Ω_ci, temperature to T_0, and electric field to B_0c.

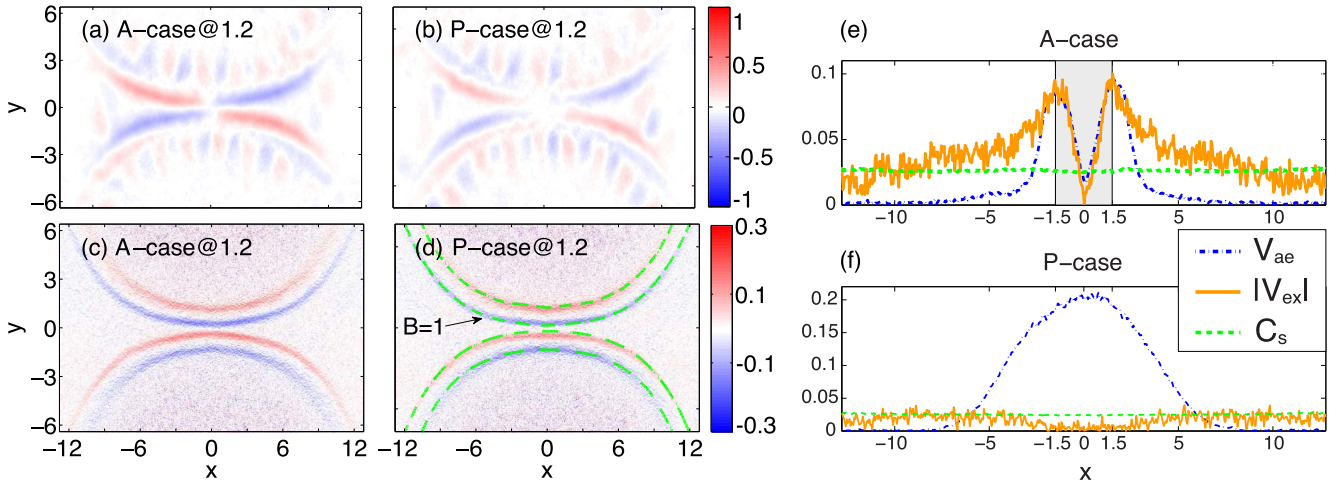

Figure 2. PIC simulation results at time $\tau = 1.2$: (a), (b) out-of-plane magnetic field B_z, (c), (d) bipolar poloidal electric field E_y, where the green dashed line indicates the magnetic field $B/B_0 = 1$. (e), (f) The electron outflow velocity v_{ex} along the line $y = 0$ for A- and P-cases, where C_s and V_{ae} are the local ion acoustic speed and electron Alfvén speed.

3. Ambiguities to identify MR

As is known, the MR process generally has many observable consequences, for instance reorganization of magnetic configurations and significant magnetic energy dissipation into heating and accelerating. However, when exploring the upcoming features in the HED regime, special care should be taken to separate these consequences from the pure influence of bubble collision effects.

To make our argument more clearly, let us see two similar contours of the electromagnetic fields in figure 2. These pictures are symptoms of the two-fluid effects—the quadrupole magnetic fields (figure 2(a)) and bipolar electric fields (figure 2(c)), which are widely accepted as important features of collisionless reconnection [1]. Nevertheless, such effects can also be driven by bubble collision effects without MR, see figures 2(b) and (d). It is not hard to understand. At the beginning, the particles (electrons and ions) around the bubble ribbon are well frozen in the magnetic field lines. Then they are pushed towards the stagnation center while the plasma bubbles are squeezed. Because the electrons are much lighter than ions, they decouple with ions gradually by shifting along the curved magnetic field lines. The process consequently leads to the out-of-plane magnetic fields B_z, i.e., the quadrupole fields in figures 2(a), (b), which is independent on the direction of the magnetic field. In other words, no matter whether reconnection occurs or not, quadrupole field, which is just a consequence of the advection of the magnetic fields by the electron flow [20, 21], will arise eventually. This can also be confirmed by the Hall bipolar electric field E_y near the stagnation region, as shown in figures 2(c), (d).

In addition, as can be noticed in figures 2(c), (d), there are extra laminar electric fields around the bubble ribbons [15]. The physical origin of these extra laminar electric fields is similar: they both result from the decoupling of electrons and ions near the magnetic ribbon when two plasma bubbles are decelerated by each other. As indicated by the green dashed line in figure 2(d), the four laminar electric fields fit the contour of the magnetic field $|\boldsymbol{B}|/B_0 = 1$ well. Moreover, the direction of this extra electric field is pointing to the expansion center. In the real HED experiments, these four electric fields will unexpectedly alter the trajectories of probing protons, therefore, it is harmful for the observation of MR by proton imaging and it may eventually affect the laboratory diagnoses of the magnetic configurations.

Besides the electromagnetic fields, the ambiguities also lay in the observation of temperature. The particle heating was regarded as evidence for MR [9, 22–24]. However, as demonstrated by [15], no considerable differences occur by comparing the control cases. Instead of showing a similar figure as in [15], we try to understand it by the physical intuition. Because of strongly driven squeezing effects, the particles bump between the piled up magnetic fields. Thus, the electrons and ions will be heated near the interaction region. In a high compression regime, it is safe to imply that stronger squeezing effects will lead to higher temperature.

While both cases show similar profiles of the EM fields and temperature, it is ambiguous to determine the dominate effects in the generation of the collimated jets observed in the previous experiments [9, 11, 12], which is because jets can also be driven by squeezing effects. To clarify this, we plot the electron velocity along the line $y = 0$ in x-direction, where $C_s \sim 0.025$ is the local ion acoustic velocity. Figure 2(e) shows clearly for the A-case, the velocity of the electron jets V_{ex} is close to the local electron Alfvén velocity $V_{ae} = B/\sqrt{\mu_0 m_e n}$ in this region $-1.5 < x < 1.5$, and drops to the ion acoustic speed C_s out of the region. For the P-case, the purely bubble collision cannot support such a strong outflow as in the A-case, where the maximum outflow is four times slower, close to the local acoustic velocity C_s. These results show that the MR effects can drive stronger jets in a highly magnetized environment, since a route should exist for the MR process to dissipate the magnetic energy. Naturally, if it is not heating, then it is accelerating.

4. Key effects of MR

Now let us turn to the key consequence of MR—the magnetic energy conversion process. We shall confirm the magnetic energy will actually dissipate in the MR case. As was pointed out in [15], a key sign of MR, i.e., an electron dissipation region, will arise in the A-case. To understand it, one always compares the PIC results with the generalized Ohm's law that follows from the electron motion [1]:

$$\boldsymbol{E} = -\boldsymbol{v}_\mathrm{e} \times \boldsymbol{B} - \frac{1}{n_\mathrm{e} e}\nabla \cdot \boldsymbol{P}_\mathrm{e} - \frac{m_\mathrm{e}}{e}\left(\frac{\partial \boldsymbol{v}_\mathrm{e}}{\partial t} + \boldsymbol{v}_\mathrm{e} \cdot \nabla \boldsymbol{v}_\mathrm{e}\right), \quad (4)$$

where the resistive term is neglected since the plasma is collisionless. For the A-case, near the colliding center, it is not hard to see the out-of-plane electric fields E_z are mainly supported by the term $\boldsymbol{v}_\mathrm{e} \times \boldsymbol{B}$. However, for the colliding center where the velocity $v_\mathrm{e} \sim 0$, the fields E_z are supported by the off-diagonal electron pressure tensor [8, 15],

$$E_z \approx -\frac{1}{ne}(\partial_x P_{exz} + \partial_y P_{eyz}), \quad (5)$$

which is a well-known result in the previous MR researches (e.g., [25]), though, which one ($\partial_x P_{exz}$ or $\partial_y P_{eyz}$) is the dominant term is still being explored in the HED regime [8, 15]. Since we are more interested in the distinguishable properties between A- and P-cases here, we refer the readers to [8, 15, 17, 18] for more detailed comparison of each fluid terms in equation (4) with the PIC results.

With the emergence of fields E_z in the A-case, the electron dissipation region (EDR) arises while the dissipation term is not zero $\boldsymbol{J} \cdot (\boldsymbol{E} + \boldsymbol{v}_\mathrm{e} \times \boldsymbol{B})$. Usually, this term is enough to distinguish the electron dissipation region while the relativistic properties are not evident in the PIC simulations. However, since the relativity is much easier to be attained by the intense laser in the HED regime, we plot the EDR in figure 3(a) to catch this characterization by a different quantity proposed in [26]. It is a Lorentz-invariant scalar quantity in the electron frame,

$$\begin{aligned} D_\mathrm{e} &= J_\mu F^{\mu\nu} u_\nu \\ &= \gamma_\mathrm{e}[\boldsymbol{j} \cdot (\boldsymbol{E} + \boldsymbol{v}_\mathrm{e} \times \boldsymbol{B}) - \rho_c(\boldsymbol{v}_\mathrm{e} \cdot \boldsymbol{E})], \end{aligned} \quad (6)$$

where J^μ, $F^{\mu\nu}$ and u^ν are the four-current, electromagnetic tensor, four-velocity, respectively, with the Lorentz factor $\gamma_\mathrm{e} = [1 - (v_\mathrm{e}/c)^2]^{-1/2}$ and the charge density $\rho_\mathrm{e} = (n_\mathrm{i} - n_\mathrm{e})e$. The component $j_z \cdot (\boldsymbol{E} + \boldsymbol{v}_\mathrm{e} \times \boldsymbol{B})_z$ mainly contributes to such a dissipation, through which the magnetic energy is reduced as indicated by the red line in figure 3(c). For the P-case, in contrast, the opposite direction of the fields E_z are cancelled out, hence, no electron dissipation region appears in figure 3(b), and the total magnetic energy $U_1 = \int B^2/(2\mu_0)\mathrm{d}\Omega$ over the whole simulation box Ω only drops slightly, which is indicated by the blue line in figure 3(c). By comparing figures 3(c) and (d), for the A-case, the decrease of total magnetic energy U_1 is mainly due to the magnetic annihilation in the xy-plane, even though, the magnetic energy $U_2 = \int B_z^2/(2\mu_0)\mathrm{d}\Omega$ over the whole simulation box Ω increases over time due to the two-fluid effects, see figure 3(d). Therefore, it is confirmed that the MR process helps to relax the free magnetic energy and launch the jets as mentioned above.

Apart from the relaxation of magnetic energy, the MR process will also lead to a relaxation of plasma density gradient. From the view of magneto-hydrodynamics, the plasma density evolves with the magnetic fields. It is not hard to imagine that the plasma density will change significantly when the MR occurs. The differences between the case with and without MR can be seen from the contours of plasma density n in figure 4, where the green lines indicate the magnetic field. For both cases at time $\tau = 1.8$, blocked by the magnetic field lines, plasmas are piled up at the up-stream, see figures 4(a) and (b). For the A-case at a later time, because of the magnetic annihilation, the plasma is no longer obstructed by the magnetic fields. As a result, plasmas in one bubble can flow freely into the other one, when two ribbons have merged into one, as shown in figure 4(c). In contrast, since no MR process occurs for the P-case in figure 4(d), plasmas are still well confined by the field lines with few differences compared with the early time. Therefore, the gradient of the plasma density is finally relaxed by the reorganization of the magnetic fields, which is solely due to the MR process.

5. Discussion and conclusion

With the simulation results of two colliding bubbles in 2D plane, we discuss two fundamentally interesting features to be studied further. One is the 3D effects, with which the magnetic fields evolve in the real experiments, since the above results are only concluded from the 2D cases. This question is inescapable in the present HED experiments. At a first attempt, we extend the 2D plane homogeneously in z-direction to get a 3D case; the two ribbons now become two half cylinders. As expected, most of the above results are nearly not affected. For instance, figure 5(a) presents a 3D view of the quadrupole fields B_z—the symptom of two-fluid effects, and reconnection configurations of magnetic fields B_x. Interestingly, differences do exist by such a simple extension from 2D to 3D. To make it more concrete, we can see an instability-like pattern arises on the xz-plane (the colliding plane $y = 0$), as shown in figures 5(c), (d), even though a little fuzzy. These expensive 3D simulations suggest the variations along the z-direction, e.g., induced by instabilities, may eventually alter the dynamics on the xy-plane. So, much more efforts are needed to get a clearer answer. In addition, to mimic the experiments setup, we also try the case: two hemisphere bubbles collide eccentrically head-on. The physical meaning is a little vague there and it also challenges the present visualization techniques in handling these complex 3D configurations. We do not report the results here, but conclude that the 3D effects in simulations have prolific features to explore, which has the enlightening significance for the explanations of experiments.

Besides the 3D effects, the relativistic feature is also challenging. As is known, the concept of reconnection in the relativistic regime is a little awkward, if one writes the transformed magnetic fields by a different observer moving

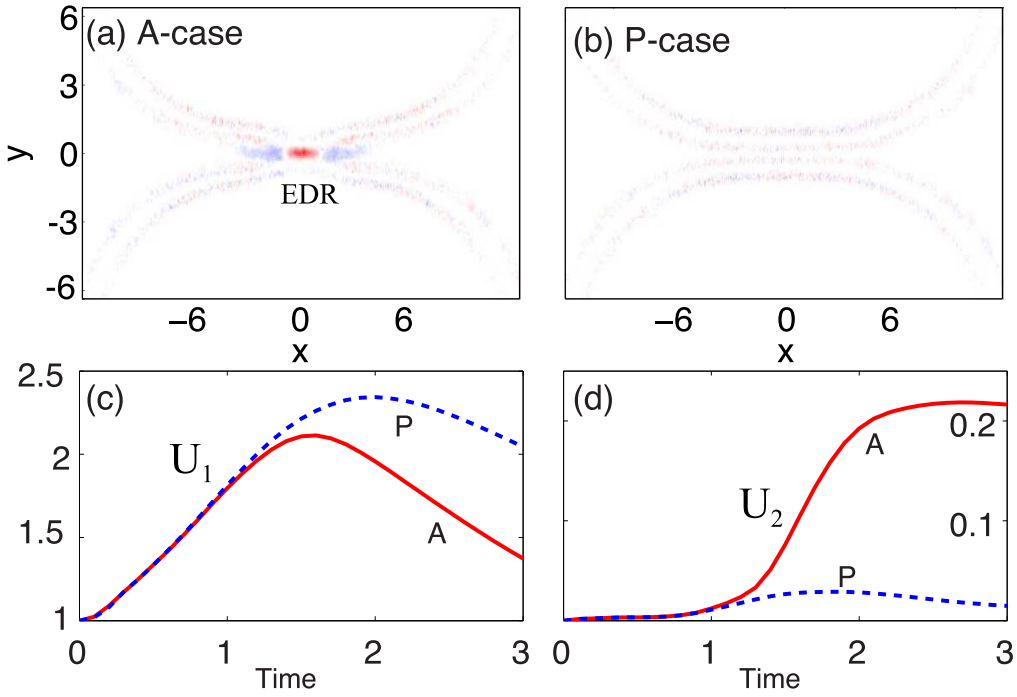

Figure 3. PIC simulation results: (a), (b) the electron dissipation region indicated by D_e at time $\tau = 1.4$, where the red color indicates positive values and blue color negative; (c), (d) the magnetic energy $U_1 = \int B^2/(2\mu_0)\mathrm{d}\Omega$ and $U_2 = \int B_z^2/(2\mu_0)\mathrm{d}\Omega$ over the whole simulation box Ω varies with time, where the blue dotted line and the red line indicate the P- and A-cases, respectively.

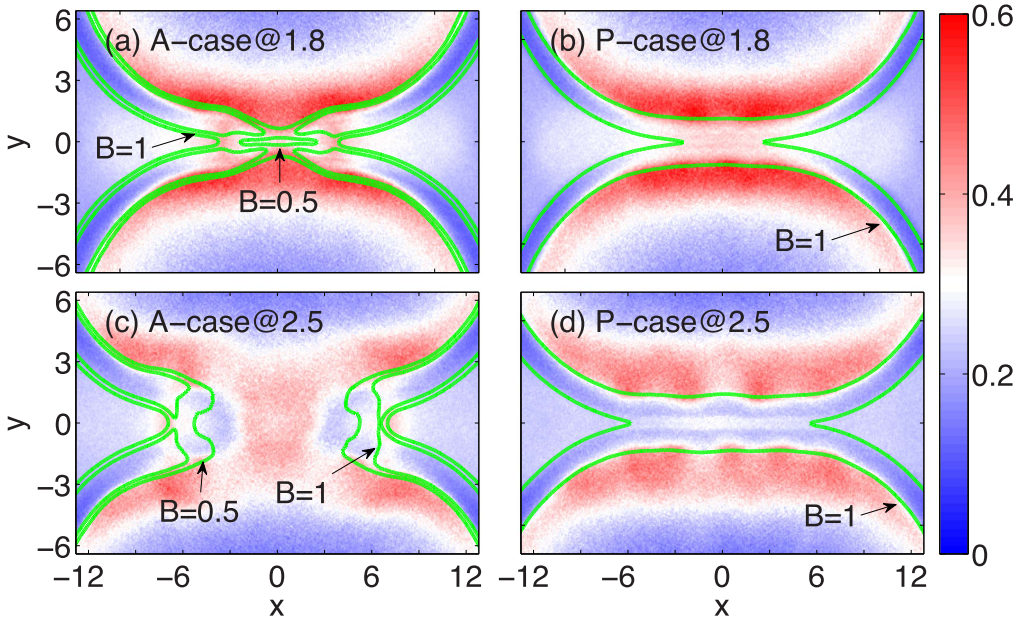

Figure 4. PIC simulation results: snapshot of density contours n/n_0: (a), (c) A-case at time $\tau = 1.8$, $\tau = 2.5$, respectively; (b), (d) P-case at time $\tau = 1.8$, $\tau = 2.5$, respectively. The green lines indicate magnetic field lines.

with a velocity v_o as,

$$\boldsymbol{B}' = \gamma_o\left(\boldsymbol{B} - \frac{\boldsymbol{v}_o \times \boldsymbol{E}}{c^2}\right) + (1 - \gamma_o)\frac{\boldsymbol{B}\cdot\boldsymbol{v}_o}{v_o^2}\boldsymbol{v}_o, \qquad (7)$$

where γ is the relevant Lorentz factor. Unfortunately, this means the notion of magnetic field lines is intrinsically non-relativistic. Therefore, in a relativistic limit, there is no simple definition of magnetic topology that behaves as intuitive as that in the non-relativistic limit [27–30]. For instance [28, 30], it requires the time to be reset to recover the standard form of the connection theorem, since the time and space are coupled with each other in the Minkowski spacetime. However, the main challenge is how to establish a bridge between these theoretical results and the numerical treatments. As always seen in previous simulation and experiments, the singular point—'magnetic null' in numerous studies is useful as an

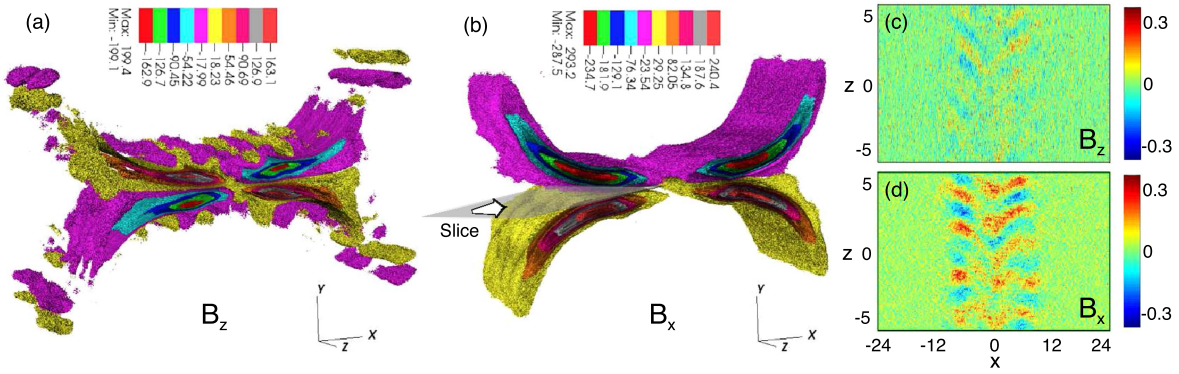

Figure 5. Magnetic fields in 3D kinetic simulations at time $\tau = 0.8$: (a), (b) the magnetic fields B_z and B_x in 3D view, respectively (c) and (d), the magnetic fields B_z and B_x on the xz-plane ($y = 0$), respectively.

indication for the reconnection events. Without such a helpful sign to tell the occurrence of MR while the X-point is not 'stable' as it used to be, it is hard to tell whether the MR happened or not. Since the intense laser is capable of driving relativistic MR events in the laboratory, the above questions of MR in the HED regime need to be answered urgently.

In summary, by simulations, we have explored the most distinguished features of MR in the HED regime such as two-fluid effects, jetting and heating. By clarifying the consequences due to the pure bubble colliding effects, we present a MR process that can convert the free magnetic energy into particles through non-thermal acceleration. With additional discussion of the 3D effects and relativistic features, the results obtained here are helpful to guide the future HED experiments for the MR process.

Acknowledgments

This work is supported by the NSAF, Grant No. U1630246; the National Key Program of S&T Research and Development, Grant No. 2016YFA0401100; the National Natural Science Foundation of China, Grants No. 11575298; the National Basic Research 973 Projects No. 2013CBA01500, and the National High-Tech 863 Project. BQ acknowledges the support from Thousand Young Talents Program of China. The computational resources are supported by the Special Program for Applied Research on Super Computation of the NSFC-Guangdong Joint Fund (the second phase).

References

[1] Yamada M, Kulsrud R and Ji H 2010 *Rev. Mod. Phys.* **82** 603
[2] Zweibel E G and Yamada M 2009 *Annu. Rev. Astron. Astrophys.* **47** 291
[3] Uzdensky D A 2011 *Space Sci. Rev.* **160** 45–71
[4] Su Y, Veronig A M, Holman G D, Dennis B R, Wang T, Temmer M and Gan W 2013 *Nat. Phys.* **9** 489
[5] Birn J, Artemyev A V, Baker D N, Echim M, Hoshino M and Zelenyi L M 2012 *Space Sci. Rev.* **173** 49
[6] Yamada M, Yoo J, Jara-Almonte J, Ji H T, Kulsrud R M and Myers C E 2014 *Nat. Commun.* **5** 4774
[7] Ji H and Daughton W 2011 *Phys. Plasmas* **18** 111207
[8] Fox W, Bhattacharjee A and Germaschewski K 2011 *Phys. Rev. Lett.* **106** 215003
[9] Nilson P M *et al* 2006 *Phys. Rev. Lett.* **97** 255001
[10] Li C K, Seguin F H, Frenje J A, Rygg J R, Petrasso R D, Town R P J, Landen O L, Knauer J P and Smalyuk V A 2007 *Phys. Rev. Lett.* **99** 055001
[11] Zhong J *et al* 2010 *Nat. Phys.* **6** 984
[12] Dong Q-L *et al* 2012 *Phys. Rev. Lett.* **108** 215001
[13] Fiksel G, Fox W, Bhattacharjee A, Barnak D H, Chang P-Y, Germaschewski K, Hu S X and Nilson P M 2014 *Phys. Rev. Lett.* **113** 105003
[14] Rosenberg M J, Li C K, Fox W, Igumenshchev I, Seguin F H, Town R P J, Frenje J A, Stoeckl C, Glebov V and Petrasso R D 2015 *Phys. Plasmas* **22** 042703
[15] Xu Z, Qiao B, Chang H X, Yao W P, Wu S Z, Yan X Q, Zhou C T, Wang X G and He X T 2016 *Phys. Rev.* E **93** 033206
[16] Arber T D *et al* 2015 *Plasma Phys. Control. Fusion.* **57** 113001
[17] Fox W, Bhattacharjee A and Germaschewski K 2012 *Phys. Plasmas* **19** 056309
[18] Lu S, Lu Q M, Dong Q L, Huang C, Wang S, Zhu J Q, Sheng Z M and Zhang J 2013 *Phys. Plasmas* **20** 112110
[19] Rosenberg M J, Li C K, Fox W, Igumenshchev I, Seguin F H, Town R P J, Frenje J A, Stoeckl C, Glebov V and Petrasso R D 2015 *Phys. Plasmas* **22** 042703
[20] Bian N H and Vekstein G 2007 *Phys. Plasmas* **14** 120702
[21] Singh N, Khazanov I and Wells B E 2015 *Phys. Plasmas* **22** 052117
[22] Phan T D, Shay M A, Gosling J T, Fujimoto M, Drake J F, Paschmann G, Oieroset M, Eastwood J P and Angelopoulos V 2013 *Geophys. Res. Lett.* **40** 4475
[23] Drake J F, Swisdak M, Phan T D, Cassak P A, Shay M A, Lepri S T, Lin R P, Quataert E and Zurbuchen T H 2009 *J. Geophys. Res. Sp. Phys.* **114** A05111
[24] Yoo J, Yamada M, Ji H T and Myers C E 2013 *Phys. Rev. Lett.* **110** 215007
[25] Pritchett P L 2001 *J. Geophys. Res. Sp. Phys.* **106** 3783
[26] Zenitani S, Hesse M, Klimas A and Kuznetsova M 2011 *Phys. Rev. Lett.* **106** 195003
[27] Hornig G and Schindler K 1996 *Phys. Plasmas.* **3** 781
[28] Pegoraro F 2012 *Europhys. Lett.* **99** 35001
[29] Pegoraro F 2016 *J. Plasma Phys.* **82** 555820201
[30] Asenjo F a and Comisso L 2015 *Phys. Rev. Lett.* **114** 115003